

EFFECTS OF EQUIVALENCE RATIO ON THE DEFLAGRATION CHARACTERISTICS PREMIXED ACETYLENE/AIR UNDER A WEAK CONSTRAINT

Bei-bei ZHANG^{a,b}, Yang-fan CHENG^{a,b,*}, Xiang LI^b, Xiao WEI^b, Jia-qi QIAN^b

^aSchool of Civil Engineering and Architecture, Anhui University of Science and Technology, Huainan,
Anhui, P. R. China

^bSchool of Chemical and Blasting Engineering, Anhui University of Science and Technology, Huainan,
Anhui, P. R. China

E-mail addresses: cyf518@mail.ustc.edu.cn (Y.-F. Cheng)

As an important energy resource, acetylene (C_2H_2) has a huge explosion risk during its production, storage and utilization processes, for the leaked C_2H_2 would easily blend with ambient air to form explosive mixtures, causing serious explosion accidents in the presence of ignition sources. A self-designed gas explosion facility were used to investigate the flame propagation behaviors and explosion characteristics of C_2H_2 /air with different equivalence ratios (ϕ) under a weak constraint. Experimental results showed that with the increasing equivalence ratio, the amount of carbon black increased, resulting in the flame colors changed from light blue to khaki, and the decay rate of the maximum explosion pressure decreased gradually. The average flame propagation velocity and flame temperature reached the maximum value of 14.16 m/s at $\phi=1.32$ and 3617 K at $\phi=1.96$, respectively. With the static placing time enlarged, the explosion pressure change trend could be divided into three stages of “falling-standing-rising”. The results would help to provide the damage data of thermal and shock wave for acetylene explosion prevention, and develop preventive measures to improve the safety of acetylene application process industry.

Key words: C_2H_2 ; gas explosion; flame propagation; flame temperature; overpressure prediction

1. Introduction

Acetylene (C_2H_2) is a type of hydrocarbon discovered by Edmund Davy in 1836, which is a favourable alternative to the conventional fossil fuels for its $C\equiv C$ with a high bond energy, releasing large amounts of heat when broken [1]. Xiu *et al.* [2] added C_2H_2 to conventional high energy fuels, which solved the problems of slow ignition and incomplete combustion, and improved its combustion efficiency. Gursharan *et al.* [3] tested the thermal efficiency of C_2H_2 fuel in the compressed ignition engine, and found that the larger flow of C_2H_2 , the higher thermal efficiency of the engine. In the context of global fossil fuel shortage and severe air pollution, it is crucial to obtain typical explosive parameters of C_2H_2 in detail for efficient and safe use of C_2H_2 . However, due to its high chemical reactivity, wide flammable range (1.5-82.2 vol.%), low ignition energy (0.019 mJ) and fast release rate of chemical reaction energy, C_2H_2 has a huge explosion risk in the processes of storage, transport and utilization, which seriously threatens personnel lives and property [4,5]. Mizutani *et al.* [6] investigated the decomposition and ignition reactions of C_2H_2 in a cylindrical closed vessel, and concluded that the lowest storage pressure of C_2H_2 at $-60\text{ }^\circ\text{C}$ was 0.18 MPa. Song *et al.* [7] studied the

explosion processes of calcium carbide dust in the C_2H_2 atmosphere using a 20 L spherical vessel, and the results showed that the explosion risk of CaC_2/C_2H_2 with the equivalence ratio of 1.78 was the greatest. Darkon *et al.* [8] measured the flame temperature of the premixed C_2H_2 /air with thermocouples in a closed burner, which was approximately the same as that measured by the two-color laser-induced incandescence. Existing studies on the explosion characteristics of C_2H_2 were mainly carried out in the confined space, while very few studies focused on its explosion characteristics in the open space. However, in the real-life production operations, C_2H_2 leaked from the storage tanks would be mixed with air to form local explosive mixtures in the open space, which may lead to serious explosion accidents when ignition sources are existed in the environment [9]. Therefore, it is of great importance to study the deflagration characteristics of C_2H_2 gas under a weak constraint.

Now, weak confinement conditions such as soap bubble and polyethylene film are commonly used to serve as the reaction vessels of unconfined gas deflagration. Kim *et al.* [10] studied the flame propagation behaviors of the combustible gas/air mixtures with soap bubbles, and concluded that the pleated flame and the increased flame velocity were caused by the combined effects of thermal diffusion instability and non-uniform concentration of the fuel-rich gas mixtures. Rokni *et al.* [11] also used soap bubbles to constrain the C_2H_2 /air mixtures, and found that the flame structure changed from smooth to honeycomb over the time, and the flame ignition rate was the highest at the equivalence ratio of 1.4. However, the size of the soap bubble was too small to well describe the flame propagation characteristics of gas clouds. As the large-scale experiments received widespread attention, a weak constraint created by the polyethylene film method was widely adopted [12]. Bao *et al.* [13] carried out deflagration experiments of methane/air at different volumes using the polyethylene film, and found that the flame propagation rate and explosion pressure of the methane/air mixture increased with the increasing volume of the reaction vessel. Tasi *et al.* [14] investigated the explosion characteristics of the premixed silane/air with different concentrations in the polyethylene films, and the experimental results showed that the variations of flame acceleration and explosion overpressure were first influenced by the concentration of the combustible gas, and followed by the sizes of the combustible gas clouds. In recent years, a weak constraint deflagration method using a latex balloon as the reaction vessel has been proposed. Compared with soap bubble and polyethylene film, the latex balloon is much easier to operate and could create an approximately isobaric condition. Acetylene mixture is a non-ideal explosive source, and the energy is not released instantaneously in the process of explosion. The flame is not affected by any external interference at the beginning of combustion, and the spherical flame propagates smoothly and stably in the balloon. Different from the 20-L exploding steel ball, the balloon expands gradually with the propagation of pressure, and the internal pressure of the balloon is in relative dynamic balance with the external environmental pressure. The whole process can be regarded as an approximate isobaric state. And the latex balloon has been well verified in the deflagration experiments of hydrogen [15], methane [16] and metal dust [17]. Otsuka *et al.* [15] studied the deflagration of premixed hydrogen/air in a 1.4 m³ latex balloon and used the brightness subtraction method to reduce the effect of ambient light to obtain clear images of flame development. Cheng *et al.* [17] conducted a series of dust experiments with transparent latex balloons to investigate the influential factors, such as dust concentration, particle size and oxygen content, on the combustion performance of TiH_2 dust clouds under the near-constant pressure conditions. Li *et al.* [16] used latex balloons to hold the flammable gas-air mixtures and proposed a new overpressure prediction model based on the steady-state flame propagation theory.

In the study, a self-designed gas explosion facility was developed to study the flame propagation and explosion characteristics of the premixed C_2H_2 /air with different equivalence ratios (ϕ). A high-speed camera was used to record the flame propagation processes, and a Python code was designed to detect the flame profile and flame propagation velocity. And the main innovation of the paper is to use the colorimetric temperature measurement technology based on blackbody radiation to calculate the distribution of transient flame temperature field. This technique could display the cloud map of flame temperature distribution in real time. The explosion pressure and its decay rate in the near field were also calculated. The results would help to provide the damage data of thermal and shock wave for acetylene explosion prevention, and develop preventive measures to improve the safety of acetylene application process industry.

2. Experimental materials and apparatus

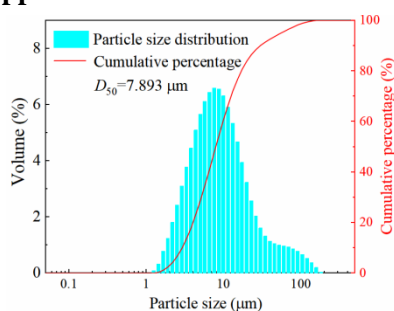


Fig. 1. Particle size distribution of tungsten wolfram powders

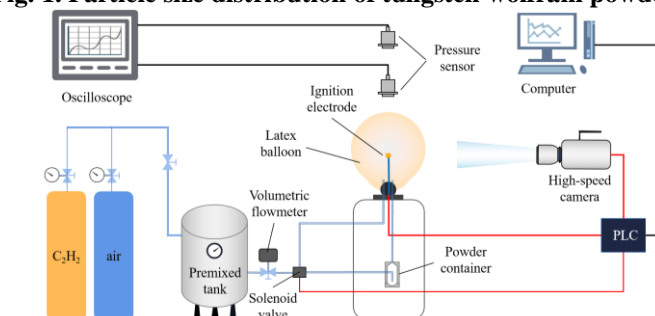
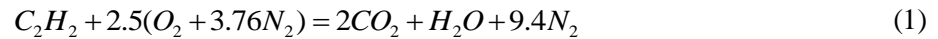


Fig. 2. Acetylene explosion test system

The experimental materials included acetylene (C_2H_2 , purity of 99.99%) and air (purity of 99.99%), which were both provided by Hefei Hang Lung Electric Technology Co., Ltd, China. The median diameter (D_{50}) of tungsten wolfram powders was ca. 7.9 μm (Shanghai Macklin Biochemical Co. Ltd, Shanghai, China), as shown in Fig. 1. Latex balloons (18 inch, Columbia) could be inflated to the maximum diameter of 45 cm. Figure 2 shows the experimental system for measuring the deflagration characteristics of premixed acetylene/air under a weak constraint. Firstly, the premixing tank was pumped to vacuum with a vacuum pump, then closed all valves and kept for 1 min to check the gas tightness. Secondly, four kinds of acetylene/air mixtures with different equivalence ratios were designed according to Dalton's law of partial pressure, where $\phi = 0.76, 1.34, 1.94, 2.61$, and the gas were filled and kept in the premixing tank for 10 min to ensure a uniform mixing. Finally, the premixed gas passed through a gas volume flow meter to fill a latex balloon until its volume reached ca. 20 L (diameter of ca. 34 cm). The premixed gases were kept in the balloon for four different time gradients of 0, 3, 6 and 9 min before being ignited by the ignition electrode of 15 kV, respectively. Explosion overpressure of the premixed gases was measured by two free-field pressure sensors (PCB 106B52 18874, sensitive: 724.81 mv/kPa, range: 0-10.0 MPa, accuracy: $\pm 99\%$. PCB 106B52 18315, sensitive: 683.8 mv/kPa, range: 0-10.0 MPa, accuracy: $\pm 99\%$. United State) placed at 2 and 4 m away

from the center of the ignition electrode, respectively. Pressure data was recorded by an oscilloscope (TELEDYNE LECROY, HDO4034, accuracy: $\pm 99.5\%$, United State) with a sampling frequency of 200 kS/s, and a high-speed camera (NAC, MEMRECAM HX-3, Japan) was used to capture the flame structure and propagation process at a frame rate of 5000 fps. The ignition electrode and data acquisition equipment (oscilloscope and high-speed camera) were controlled by a programmable logic controller (PLC, uncertainty: 0.5%), and the experiments were carried out at the ambient temperature and pressure. Because the error of the equipment is small and basically negligible, the paper does not analyze the error generated by the equipment and instruments.

The complete reaction equation of C_2H_2 and air can be expressed as follows:



Equivalence ratio (φ) was used to express the volume proportion of C_2H_2 in the gas mixtures and could be calculated by the following equation:

$$\varphi = \frac{n}{n_{st}} \quad (2)$$

where n represented the actual ratio of C_2H_2 volume fraction to air volume fraction and n_{st} represented the ratio under the stoichiometric concentration.

Table 1. C_2H_2 /air equivalence ratios in the experiments

Experimental condition	C_2H_2 (Vol.%)	air (Vol.%)	Equivalence ratio (φ)
1	6	94	0.76
2	10	90	1.32
3	14	86	1.94
4	18	82	2.61

The main influence factor of gas explosion included gas equivalence ratios, so the paper mainly focused on the study of C_2H_2 /air premixed gases under different equivalence ratios. Table 1 shows the equivalence ratios of C_2H_2 /air in the experiments, and $\varphi < 1$ indicated that the complete reaction was fuel-lean, while $\varphi > 1$ indicated that the complete reaction was fuel-rich. Bivol *et al.* [18] found that the patterns of the flame propagation at the atmospheric pressure were closed to the real technological conditions when the equivalence ratio was at fuel-lean. Previous studies had proved that the fastest flame propagation velocity of the premixed C_2H_2 /air under the weak constraint was obtained at $\varphi = 1.32$ [19]. Therefore, in the study, four equivalence ratios ($\varphi = 0.76, 1.32, 1.94$ and 2.61) of the premixed C_2H_2 /air were chosen, and each sample was tested at least three times to reduce the experimental errors.

3. Results and discussions

3.1. Flame structures in a weak constraint

The experiments were carried out in dark conditions without any interference from the external light sources, and a high-speed camera was used to record the flame propagation processes of the premixed C_2H_2 /air. As shown in Fig. 3, as the premixed C_2H_2 /air with $\varphi = 1.32$ was ignited, with the ignition electrode as the center, the combustion flame front propagated gradually outward as a spherical shape. In the time range of 0-5.6 ms, the spherical flame spread smoothly and stably inside the balloon, and the influence of external disturbance was relatively small for the balloon did not expand obviously,

and the whole process could be regarded as a laminar combustion stage. At the moment of 7.4 ms, the flame gradually destabilized from a smooth shape to a cellular shape for the hydrodynamic instability [20], and the balloon expanded subsequently with the flame expansion. Until the flame front reached the balloon wall, The flame propagation was not disturbed until the flame front reached the balloon wall, which was approximately regarded as isobaric. At the moment of 8.2 ms, the leading edge of the flame was strongly disturbed when the inner wall of the latex balloon began to rupture, and the flame color changed from blue to yellow ($t=8.6$ ms). At the moment of 10.2 ms, the latex balloon was completely ruptured and then the unburned gas was mixed with the ambient air, leading to a brighter and more violent yellow flame due to the turbulence caused by the balloon explosion.

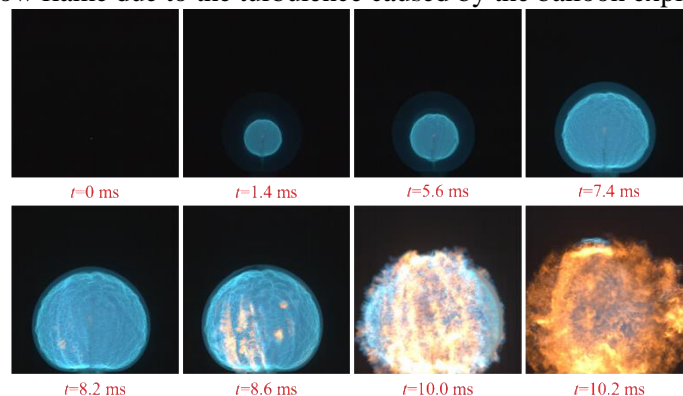


Fig. 3. Flame propagation processes of premixed C_2H_2 /air gases with ϕ of 1.32

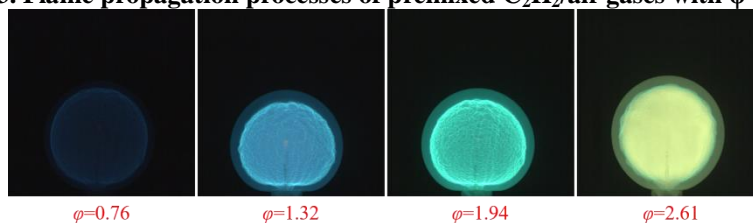


Fig. 4. Flame morphology of premixed C_2H_2 /air gases with different ϕ

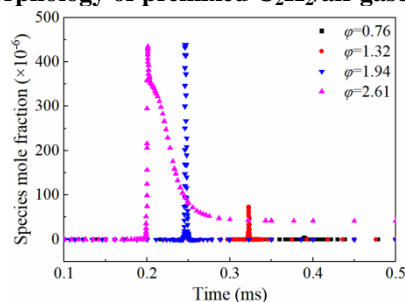


Fig. 5. Time history curves of carbon species mole fractions with different ϕ using the Chemkin software

High-speed images of the premixed C_2H_2 /air flames with four different equivalence ratios at an equal horizontal diameter were selected. As shown in Fig. 4, in the fuel-lean state ($\phi = 0.76$), the flame appeared as a pale blue oxide flame with shallow brightness and unclear cellular structure on the surface. In the fuel-rich state, the flame color changed from blue to cyan and then to khaki as the equivalence ratio increased from 1.32 to 2.61. When $\phi = 0.76$, 1.32 and 1.94, the flame color is the same as that in reference 19^[19]. Figure 5 shows the results of carbon element derived from the Chemkin simulations (Mechanism: GRI-Mech 3.0, Model: closed homogeneous 0-D reactor. The categories of the input data were “volume ratio of acetylene to air”, “total volume of the premixed gases” and “temperature and pressure of the experiment”.) [21], that is, larger amounts of carbon black would be produced as the C_2H_2 content continued to increase [7], which had a great effect on the flame

color of the C_2H_2 /air combustion. When φ was 1.32 or 1.94, carbon black was produced instantaneously and consumed by the oxygen of the premixed gases. However, when φ was 2.61, the amount of carbon black was consumed and the remaining one would produce radiation inside the balloon [11], causing the flame to be brighter in colour, which made it more difficult to observe the cellular structure on the flame surface.

3.2. Flame propagation characteristics under a weak constraint

To calculate the flame propagation velocity, a self-written Python code was applied for the flame contour detection of the high-speed images recorded by the high-speed camera. The original image captured by the high-speed camera is converted into 8-bit grayscale image, and then the grayscale image is filtered by the Open CV library in Python. In order to make the image display a more obvious contrast effect, the filtered image is binarized. The Sobel operator in Open CV library is used for edge detection. For the gas flames, the outermost continuous contour was chosen as flame front, and the re-drawn contour would only contain the external point sets without the internal texture, as shown in Fig. 6.

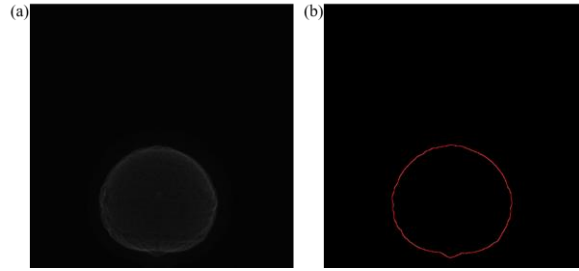


Fig. 6. Flame images processing: (a) binarization; (b) contour detection

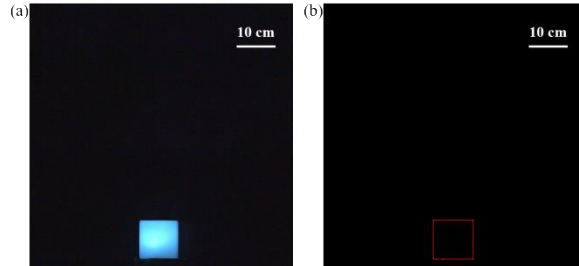


Fig. 7. Length proportional calibration: (a) real product photo; (b) contour detection chart

It should be noted that the length of the contour obtained via Python code was pixel length in the high-speed image and the true length could be obtained through calibration experiments. As illustrated in Fig. 7, the calibration experiment used a square blue lamp as the reference object, whose true side length (L_t) could be measured. Contour detection and calculation were performed on the captured image to obtain its pixel edge length (L_p). The calibration factor was expressed as the ratio of the true edge length L_t to the pixel edge length L_p , as described in Eq. (3):

$$k = \frac{L_t}{L_p} \quad (3)$$

The flame propagation velocity (S_n) was the most direct parameter to characterize the flame propagation process, which could be expressed as the change rate of flame radius with time, as shown in Eq. (4):

$$S_n = \frac{dr}{dt} \quad (4)$$

where S_n represented the flame propagation velocity, r represented the flame radius, and t represented

the time elapsed to reach that flame radius.

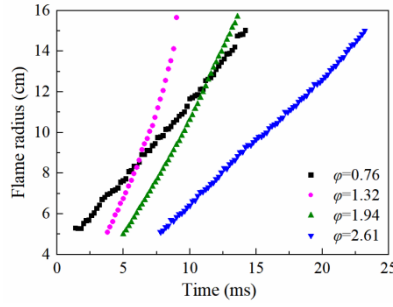


Fig. 8. Variation of C_2H_2 /air flame radius with time of different ϕ .

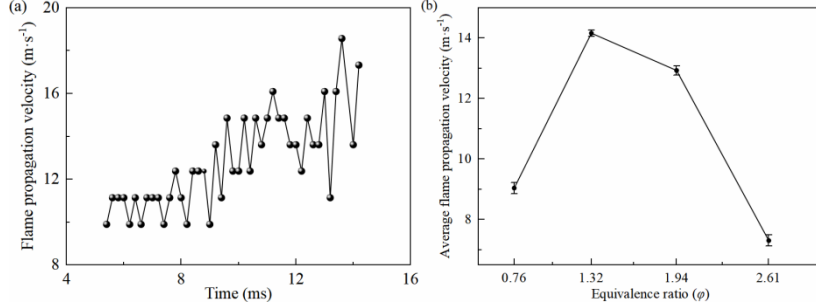


Fig. 9. Flame propagation velocity: (a) premixed C_2H_2 /air gases with $\phi=1.94$; (b) average values with different ϕ

To ensure the measurement accuracy of the facility, the shooting conditions, such as distance between the object and the high-speed camera, the focal length and the parameters setting of the camera should be the same in both calibration and gas explosion experiments. Figure 8 shows the variations of C_2H_2 /air flame radius with time for different equivalence ratios. In order to reduce the effects of spark ignition on the flame stability in the initial combustion phase, flame radius in the range of 5-15 cm were selected for analysis [22], during which the spherical flame propagated smoothly and steadily for the relatively small external disturbance (a laminar combustion stage). As shown in Fig. 8, the flame propagation radius increased approximately linearly with time in the range of 5-15 cm.

Figure 9(a) shows the variation of flame propagation velocity (S_n) with time for the premixed C_2H_2 /air at $\phi=1.94$. S_n fluctuated due to the feedback effect between the energy balance of gas molecules in the preheating zone and the flame propagation [23]. During the flame propagation, the main heat transfer forms of gas molecules were thermal radiation in the combustion zone as well as the thermal convection in the combustion zone and unburned zone. When S_n was high, the heating time for the gas molecules in the preheating zone was insufficient and part of the heat would be absorbed by the unburned gas molecules inside the flame, resulting in a reduced S_n . Subsequently, the gas molecules in the preheating zone would have sufficient time to be heated for the combustion, so S_n continued to increase. After that phase, S_n decreased again and the cycle repeated until the gas burnt out, resulting in a “fluctuated rise” of S_n . Therefore, the average flame propagation velocities of the premixed C_2H_2 /air with four different equivalence ratios were selected for analysis.



Figure 9(b) shows the average flame propagation velocity (S_a) of the premixed C_2H_2 /air increased at first and then decreased with the increasing equivalence ratios. This is consistent with the rule of reference 19^[19], the maximum value of S_a was obtained at $\phi=1.32$, which was approximately twice as large as that at $\phi=2.61$. According to the time history curves of H species mole fractions in the

premixed C_2H_2/air calculated by the Chemkin software in Fig. 10, the content of H species kept growing with the enlarged ϕ value, resulting in the increase of flame propagation velocity. However, at ϕ values of 1.94 and 2.61, Figs. 11(a) and (b) show C_2H_2 underwent mainly incomplete combustion reaction of Eq. (6) to produce CO, accompanying with the decomposition reaction of Eq. (7) to produce carbon black (as illustrated in Fig. 5). And the inhibiting effects of them were much higher than the promoting effect of the H species on the flame propagation [24], so the flame propagation velocity gradually slowed down.

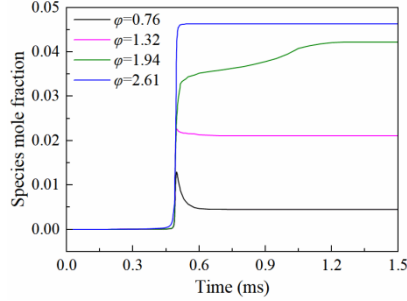


Fig. 10. Time history curves of H species mole fractions in the premixed C_2H_2/air gases with different ϕ

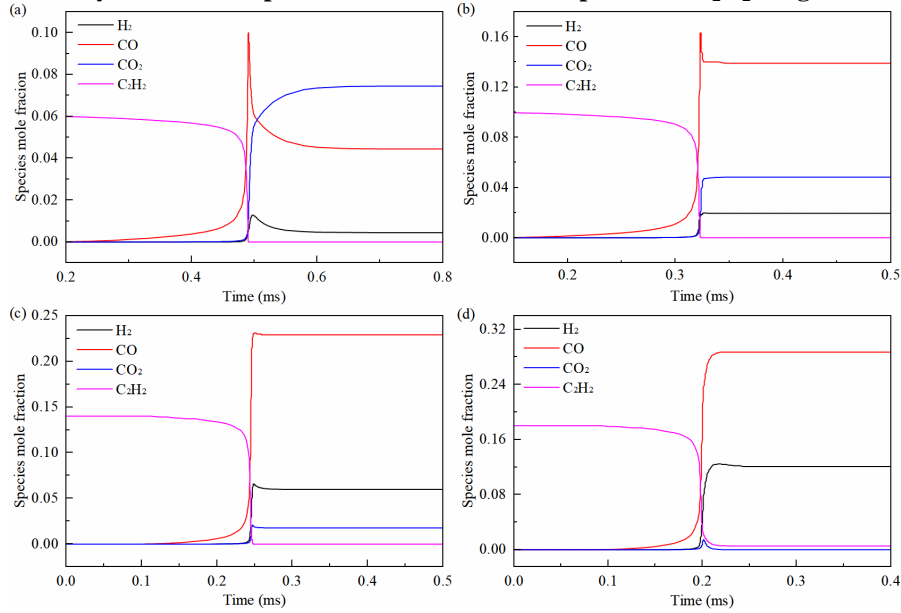


Fig. 11. Time history curves of species mole fractions in the premixed C_2H_2/air gases with different ϕ : (a) $\phi=0.76$, (b) $\phi=1.32$, (c) $\phi=1.94$; (d) $\phi=2.61$

3.3. Flame temperature distribution under a weak constraint

The deflagration thermal effect of combustible gases is also a significant cause of casualties. As a key parameters to evaluate the explosion output characteristics, temperature could reflect its thermal damage performance. Therefore, it is of great significance to carry out research on the gas flame temperature. In recent years, with the continuous maturity of photoelectric technology, non-contact optical temperature measuring methods have been developed rapidly, among which the colorimetric thermometry method is the most popular method for it does not need to determine the optical properties (such as transmittance and emissivity) of the flame before the temperature measurement [25]. Owing to the fact that there are few materials that could be served as black-body in the gas phase explosion, it is difficult to measure the flame temperature directly with the colorimetric thermometry method. In our previous study, suspended tungsten wolfram powders were chosen as the auxiliary black-body materials in gas combustion for temperature measuring [26], and the experimental system is shown in Fig. 2. At the beginning of the experiment, 0.2 g tungsten wolfram powders were put into

the powder container, and then tungsten wolfram powders were injected into the latex balloon via the premixed C_2H_2/air of a high pressure (0.15 MPa and 1.0 s spraying time), and the ignition delay time was set to be 80 ms. Furthermore, a high-speed camera was activated to capture the entire flame propagation processes of the premixed C_2H_2/air , and the transient flame temperature distribution was rebuilt by a self-written Python code.

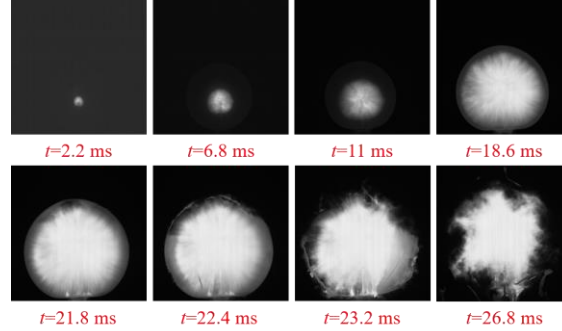


Fig. 12. Grey images of the premixed C_2H_2/air gases at $\phi=0.76$ during the flame propagation

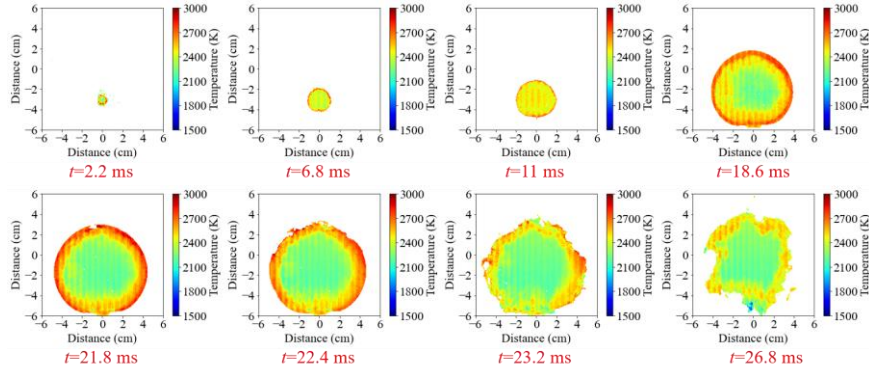


Fig. 13. Flame propagation transient temperature field distribution of the premixed C_2H_2/air

Figure 12 shows the gray images of the premixed C_2H_2/air at $\phi=0.76$ during the flame propagation. A Hamilton interpolation algorithm [27] written in the Python code was used to process the gray images and rebuild the temperature distribution maps of the flames. Figure 13 shows the temperature distribution of the premixed C_2H_2/air at $\phi=0.76$. Because the flame brightness is too shallow in the early stage of flame combustion, the pixel points cannot be detected, so the flame propagation image after $t=2.2$ ms was analyzed in the paper. In the early stages of the flame development ($t=2.2-11$ ms), the flame propagated in a nearly laminar flow (discussed in Section 3.1) with a relatively uniform temperature distribution (2300-2500 K). In the time range of 11-22.4 ms, the flame in the balloon was spherical and spread outward, and the temperatures of the spherical outer flame were higher than those of the internal flame and flame core. The reason for above phenomenon was that the internal gas combustion could continuously supply heat to the flame front along the propagation direction, and there were mainly combustion products inside the flame. Compared to the interior zone, C_2H_2 around the flame front would contact with more oxygen, which would result in a higher temperature at the flame front during the combustion [28]. At the time of 21.8 ms, a gap appeared in the upper part of the temperature map as the flame touched the inner wall of the latex balloon, causing the balloon to rupture, and the flame suddenly disappeared at this part (as shown in Fig. 12). After $t=21.8$ ms, the latex balloon started to burst and the unburned C_2H_2 would blend with the ambient air quickly, then the temperature of the outer flame dropped from ca. 2700 K to ca. 2500 K for the decreased C_2H_2 concentration and the heat exchange with the environment. The balloon ruptured completely at $t=26.8$ ms, and the flame zone shrank largely and the outer flame temperatures continued to decrease for the

lack of C_2H_2 . Furthermore, in the late combustion stage (23.2-26.8 ms), the temperatures of the outer flame tended to be equal to those of the inner flame (2300-2500 K), and much higher than those of the flame core (2050-2250 K).

Figure 14 shows the maximum flame average temperatures of the premixed C_2H_2 /air calculated by Chemkin and colorimetric thermometry at $\phi=0.76, 1.32, 1.94$ and 2.62 , respectively. The maximum flame average temperatures obtained from the Chemkin simulations were 2534, 3235, 3617 and 3279 K, respectively. When $\phi < 1$, a complete combustion reaction of Eq. (5) occurred, and the flame temperature was relatively low due to the poor concentration of C_2H_2 . When $\phi > 1$, C_2H_2 reached a certain concentration at which the oxygen content began to be insufficient, and the reaction transitioned to Eq. (6), and reactions as shown in Eqs. (5) and (6) co-occurred in the container, resulting in more heat releasing. Hydrogen content gradually went up as the value of ϕ increased, and the flame temperature would rise for the significant thermal effect of hydrogen. However, when ϕ continued to increase, the oxygen content was seriously insufficient and some C_2H_2 underwent the decomposition reaction of Eq. (7), so the heat released by the reaction and flame temperature both began to decrease.

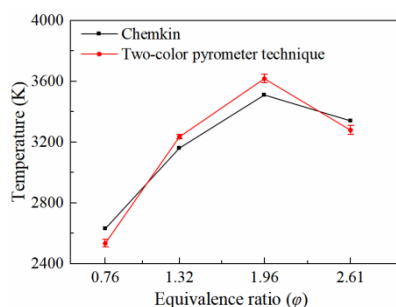


Fig. 14. Maximum flame average temperatures of the premixed C_2H_2 /air with different equivalence ratios

3.4. Explosion overpressure characteristics of C_2H_2 /air

Explosion overpressure (ΔP) is a critical parameter in evaluating the consequences of an accident and establishing relevant protective measures [29], which were recorded at 2 and 4 m away from the explosion center in an open field. Fig. 15 shows the time curves of explosion pressure and pressure rise rate of the premixed C_2H_2 /air at $\phi=1$. The explosion pressure evolution process could be divided into four stages [30]: (I) Pressure constant stage, where the explosion pressure inside the latex balloon maintained at the initial state. (II) Pressure build-up stage, where the explosion pressure came to the maximum value for the exothermic combustion, while the overpressure rise rate increased at first and then gradually decreased to zero. (III) Pressure drop stage, where after the explosion pressure reached its maximum value, it began to drop to the lowest point of pressure (negative value). (IV) Oscillation stage [31], where strong disturbance of the surrounding was formed by the balloon rupture, which made the gas explosion pressure fluctuated.

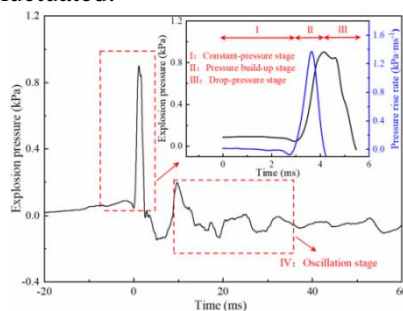


Fig. 15. Different evolution stages of explosion pressure of the premixed C_2H_2 /air gases

3.4.1 Influence of static placing time

In the gas explosion experiments, static placing is usually used to ensure that the gas mixtures remain homogeneous and stationary before ignition. In the study, the explosion characteristics of the premixed C₂H₂/air with 4 kinds of different static placing time of 0, 3, 6 and 9 min were investigated. As shown in Fig. 16, the maximum explosion overpressure (ΔP_{\max}) of the premixed C₂H₂/air with different ϕ measured at 2 and 4 m followed the same trend as the static placing time increased, which could be divided into three stages of “falling-standing-rising”. In the first stage, ΔP_{\max} of the premixed gases showed a significant decrease as the static placing time rose from 0 to 3 min, and the maximum decrease occurred at 2 and 4 m away from the ignition center with the same ϕ of 1.94, which were reduced by 36.28% and 46.51%, respectively. When the static placing time was 0 min, the initial high turbulence resulted in a large ΔP_{\max} value, and then decreased sharply as the turbulence decayed with the static placing time. In the second stage, the static placing time was enlarged from 3 to 6 min and ΔP_{\max} showed a slight increasing trend, which should be attributed to the combined effects of decayed turbulence and enhanced blend uniformity [32]. In the third stage, the effect of turbulence could be neglected, and ΔP_{\max} strengthened as the static placing time extended from 6 to 9 min, and the maximum rise occurred at 2 m away from the ignition center for $\phi=2.61$ (increased by 60.71%) and 4 m for $\phi=1.32$ (increased by 70.69%), respectively. The main reason for the above experimental results was that the static placing time was too long, then the mixtures would be stratified due to the action of gravity, which made the heterogeneity of the premixed gases more clearly, leading to the higher explosion parameters of non-uniform mixtures than those of uniform ones [33]. In general, the optimum static placing time for the premixed C₂H₂/air explosion laminar combustion was 3-6 min. And the premixed gases would present a better mixing uniformity and a lower turbulence intensity during this period, which were beneficial to obtain optimal explosion parameters.

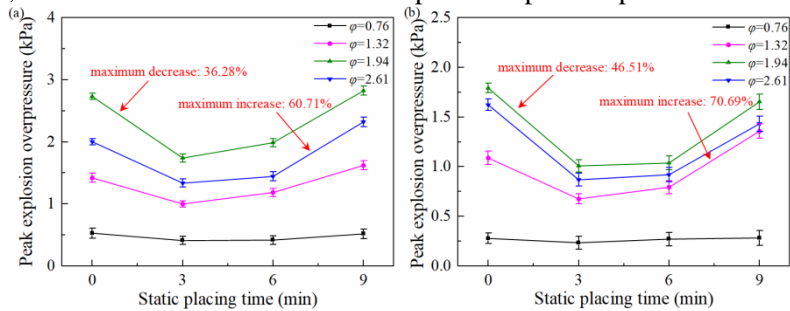


Fig. 16. Effects of static placing time on the explosion overpressure of the premixed C₂H₂/air gases with different ϕ measured at: (a) 2 m; (b) 4 m

3.4.2 Influence of equivalence ratios

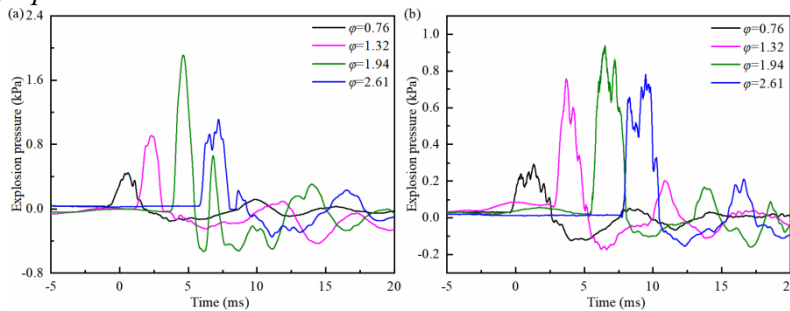


Fig. 17. Explosion pressure time curves of the premixed C₂H₂/air gases with different ϕ at (a) 2 m; (b) 4 m

Based on the experimental results mentioned above, the C₂H₂/air mixtures were kept in the balloon for 6 min and the explosion pressure time curves are shown in Fig. 17. The explosion overpressure ΔP tended to rise at first and then fall over the time, reaching ΔP_{\max} of 1.98 and 1.46 kPa both at the 2 and

4 m positions with $\varphi=1.94$, respectively. ΔP_{\max} followed the same change trends as the maximum flame temperatures at different equivalence ratios, and they both reached the maximum values at $\varphi=1.94$. As shown in Fig. 18, the decay rate of the peak pressure decreased as the equivalence ratio increased, that is, 52.54%, 33.61%, 26.26% and 23.13%, respectively. Analysis suggested that when the balloon ruptured, the unburned premixed gases would suddenly leak and mix with the ambient air, and the explosion intensity was weak when the fuel-lean balloon burst, whereas much stronger as the fuel-rich balloon burst for the higher concentration of C_2H_2 would blend with air again, and the gas explosion overpressure would affected a much wider zone [34].

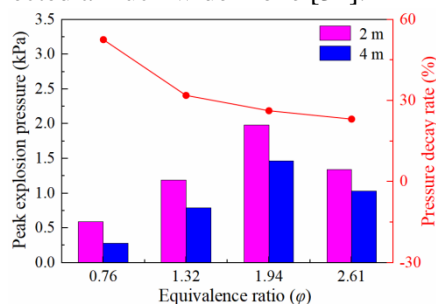


Fig. 18. Peak pressure and pressure decay rate under different φ

4. Conclusions

In the study, the flame behaviors and explosion characteristics of the premixed C_2H_2 /air were studied and some important conclusions were obtained. At the beginning of the flame propagation, the spherical flame surfaces of the premixed C_2H_2 /air were smooth, and the hydrodynamic instability effect was enhanced as the flame radius increased, resulting in the instability of flame structure and the appearance of cellular lattice structure on the flame surface. With the increasing equivalence ratio, the carbon black produced by the gas combustion gradually increased and the flame color changed from light blue, blue, cyan to khaki, and the average flame propagation velocities at the four equivalence ratios were 9.04, 14.16, 12.83 and 7.31 m/s, respectively.

The transient gas flame temperature distributions measured by the improved colorimetric thermometry with suspended tungsten wolfram powders showed that, as the premixed C_2H_2 /air flame propagated, the temperatures of the outer flame were much higher than the temperatures of the inner flame and the flame core when the balloon was undamaged, but the temperatures of the outer flame tended to be equal to those of the inner flame after the balloon was burst, and they were both higher than those of the flame core. The average temperatures of gas flames tended to increase and then decrease with the increasing equivalence ratios, reaching a maximum value of 3617 K at $\varphi=1.94$.

With the propagation of the spherical flame, the explosion overpressure went through four phases of pressure constant stage, pressure build-up stage, pressure drop stage and oscillation stage. The explosion overpressure rose at first and then decreased with the increasing equivalence ratios, and the maximum explosion overpressure occurred at $\varphi=1.94$. ΔP_{\max} of the premixed C_2H_2 /air with 4 kinds of equivalence ratios were decayed from 2 to 4 m by 52.54%, 33.61%, 26.26% and 23.13%, respectively. With the extension of the static placing time, ΔP_{\max} could be divided into three stages of “falling-standing-rising”.

Acknowledgements

Many thanks to Prof. Ritsu Dobashi, Assoc. Prof. Toshio Mogi and Dr. Po-Jul Chang of the University of Tokyo, for their kindness help with the two-color pyrometer technique. The work was supported by the Distinguished Youth Project of University Natural Science Foundation of Anhui

Province (No. 2023AH020026), the National Natural Science Foundation of China (No.12272001) and Anhui New Era Education Quality Project (No. 2023xscx071), and the authors would like to thank these foundations for the financial supports.

References

- [1] Schobert, H. Production of acetylene and acetylene-based chemicals from coal, *Chemical Reviews*, 114 (2014), pp. 1743-1760.
- [2] Xiu-tian-feng, E., *et al.* Acetylene solubility in high-energy-density fuels enhanced by amines and scrambled cages, *Chemistry and Technology of Fuels and Oils*, 54 (2018), pp. 599-605.
- [3] Singh, G., *et al.* Optimization of performance, combustion and emission characteristics of acetylene aspirated diesel engine with oxygenated fuels: An Experimental approach, *Energy Reports*, 7 (2021), pp. 1857-1874.
- [4] Wu, Y., *et al.* An experimental study on the detonation transmission behaviours in acetylene-oxygen-argon mixtures, *Energy*, 143 (2018), pp. 554-561.
- [5] Voronin, V. V., *et al.* Acetylene in organic synthesis: Recent progress and new uses, *Molecules*, 23 (2018), 2442.
- [6] Mizutani, T., *et al.* Decomposing deflagration properties of acetylene under low temperatures, *Journal of Loss Prevention in the Process Industries*, 20 (2007), pp. 688-690.
- [7] Song, S. X., *et al.* Explosion behaviors of hybrid C₂H₂/CaC₂ dust in a confined space, *Journal of Hazardous Materials*, 416 (2021), 125783.
- [8] Drakon, A. V., *et al.* Optical properties and structure of acetylene flame soot, *Applied Physics B*, 127 (2021), 81.
- [9] Atkinson, G., *et al.* A review of very large vapour cloud explosions: Cloud formation and explosion severity, *Journal of Loss Prevention in the Process Industries*, 48 (2017), pp. 367-375.
- [10] Kim, W. K., *et al.* Effect of propagation behaviour of expanding spherical flames on the blast wave generated during unconfined gas explosions, *Fuel*, 128 (2014), pp. 396-403.
- [11] Rokni, E., *et al.* Measurement of laminar burning speeds and investigation of flame stability of acetylene (C₂H₂)/air mixtures, *Journal of Energy Resources Technology*, 137 (2015) .
- [12] Bull. D. C. Review of large- scale explosion experiments, *Plant/Operations Progress*, 11 (1992), pp. 33-40.
- [13] Bao, Q., *et al.* Experimental investigation on the deflagration load under unconfined methane-air explosions, *Fuel*, 185 (2016), pp. 565-576.
- [14] Tsai, H. Y., *et al.* Unconfined silane-air explosions, *Journal of Loss Prevention in the Process Industries*, 49 (2017), pp. 700-710.
- [15] Otsuka, T., *et al.* Hazard evaluation of hydrogen-air deflagration with flame propagation velocity measurement by image velocimetry using brightness subtraction, *Journal of Loss Prevention in the Process Industries*, 20 (2007), pp. 427-432.
- [16] Li, M., *et al.* Flame propagation characteristics and overpressure prediction of unconfined gas deflagration, *Fuel*, 284 (2021), 119022.
- [17] Cheng, Y. F., *et al.* Flame propagation behaviors and influential factors of TiH₂ dust explosions at a constant pressure, *International Journal of Hydrogen Energy*, 43 (2018), pp. 16355-16363.
- [18] Bivol, G. Y., *et al.* Investigation of hydrogen-air and acetylene-air flame propagation through porous media using infrared visualisation, *Process Safety and Environmental Protection*, 163 (2022), pp. 368-383.

- [19] Wang, W. T., *et al.* Flame behaviors and overpressure characteristics of the unconfined acetylene-air deflagration, *Energy*, 246 (2022), 123380.
- [20] Kim, W., *et al.* Experimental investigation on the onset of cellular instabilities and acceleration of expanding spherical flames, *International Journal of Hydrogen Energy*, 42 (2017), pp. 14821-14828.
- [21] GREGORY, P., SMITH, D. G. GriMech 3.0, (2005/2007).
- [22] Hanai, H., *et al.* A numerical study of pulsating flame propagation in mixtures of gas and particles, *Proceedings of the Combustion Institute*, 28 (2000), pp. 815-822.
- [23] Rubtsov, N. M., *et al.* Interaction of the combustion front of methane-air mixture at low pressures with obstacles of cylindrical shape, *FirePhysChem*, 1 (2021), pp. 174-178.
- [24] Slavinskaya, N., *et al.* A modelling study of acetylene oxidation and pyrolysis, *Combustion and Flame*, 210 (2019), pp. 25-42.
- [25] Wang Z. H., *et al.* Flame structures and particle-combustion mechanisms in nano and micron titanium dust explosions, *Journal of Loss Prevention in the Process Industries*, 80 (2022), pp. 104876
- [26] Cheng, Y. F., *et al.* An improved two-colour pyrometer based method for measuring dynamic temperature mapping of hydrogen-air combustion, *International Journal of Hydrogen Energy*, 46 (2021), pp. 34463-34468.
- [27] Adams Jr., J.E., Hamilton Jr., J.F. Adaptive Color Plane Interpolation in Single Sensor Color Electronic Camera, U.S., New York. (1997), Patent Number: 5652621.
- [28] Chang, P. J., *et al.* An investigation on the dust explosion of micron and nano scale aluminium particles, *Journal of Loss Prevention in the Process Industries*, 70 (2021), pp. 104437.
- [29] Zhu, Y., *et al.* Investigation on the overpressure of methane-air mixture gas explosions in straight large-scale tunnels, *Process Safety and Environmental Protection*, 135 (2020), pp. 101-112.
- [30] Li, Y., *et al.* Explosion hazard evaluation of renewable hydrogen/ammonia/air fuels, *Energy*, 159 (2018), pp. 252-263.
- [31] Sun, S., *et al.* Effects of concentration and initial turbulence on the vented explosion characteristics of methane-air mixtures, *Fuel*, 267 (2020), 117103.
- [32] Lawes, M., *et al.* Influence of spark ignition in the determination of Markstein lengths using spherically expanding flames, *Fuel*, 186 (2016), pp. 579-586.
- [33] Zhang, Z., *et al.* Investigation on flame characteristics of industrial gas turbine combustor with different mixing uniformities, *Fuel*, 259 (2020), 116297.
- [34] Huang, Y., *et al.* Estimation of the Fireball Size in an Ethyne-Air Cloud Explosion, *Combustion, Explosion, and Shock Waves*, 54 (2018), pp. 106-112.

Submitted: 11.11.2024.

Revised: 14.01.2025

Accepted 20.01.2025.